

# Computing the graph-changing dynamics of loop quantum gravity

T. L. M. Guedes,<sup>1,2,\*</sup> G. A. Mena Marugán,<sup>3,†</sup> F. Vidotto,<sup>3,4,‡</sup> and M. Müller<sup>1,2,§</sup>

<sup>1</sup>*Institute for Quantum Information, RWTH Aachen University, D-52056 Aachen, Germany*

<sup>2</sup>*Peter Grünberg Institute, Theoretical Nanoelectronics,  
Forschungszentrum Jülich, D-52425 Jülich, Germany*

<sup>3</sup>*Instituto de Estructura de la Materia, IEM-CSIC, C/ Serrano 121, 28006 Madrid, Spain*

<sup>4</sup>*Department of Physics and Astronomy, Department of Philosophy,  
and Rotman Institute, Western University, N6A 5B7, London, Ontario, Canada.*

In loop quantum gravity (LQG), quantum states of the gravitational field are represented by labelled graphs called spinnetworks. Their dynamics can be described by a Hamiltonian constraint, which modifies the spinnetwork graphs. Fixed graph approximations of the dynamics have been extensively studied, but its full graph-changing action so far remains elusive. The latter, alongside the solutions of its constraint, are arguably the missing features to access physically correct quantum-relativistic phenomenology from canonical LQG. Here, we introduce the first numerical tool that implements graph-changing dynamics via the Hamiltonian constraint. We find new solutions to this constraint and show that some quantum-geometrical observables behave differently than in the graph-preserving truncation. This work aims at fostering a new era of numerical simulations in canonical LQG that, crucially, embrace the graph-changing aspects of its dynamics, laying aside debated approximations.

Loop quantum gravity (LQG) is a tentative quantum theory of gravity with the distinct feature of geometric observables having discrete spectra [1]. While its mathematics is fairly well defined, computations are extremely challenging. Recently, numerical computations [2–6] were achieved within the covariant formulation of the theory [7], yet none of these numerical tools apply to the canonical approach [8]. The dynamics of canonical LQG is defined by a single operator, the Hamiltonian constraint [9]. It acts on a state space for the quantum spacetime geometry that admits a basis labeled by spinnetworks (SNs) [10, 11]. These are closely related to ribbon-graphs and string-nets [12–14]. SNs are graphs with spins assigned to links, and nodes forming singlets out of the link spins [15–18]. The Hamiltonian-constraint action on a SN changes the graph and its spin assignments in multiple ways, yielding a large superposition of SNs with different graphs. This complication is amplified by the quantum-volume operator in the Hamiltonian. Calculating matrix elements of the volume requires diagonalizing matrices built on subspaces of SNs with identical graphs, which demands numerical approaches largely lacking in canonical LQG. The resulting dynamics, as well as the solutions to its constraint, have therefore remained inaccessible. Even its effect on the volume – a key observable to extract information about the (quantum) geometry – has yet to be characterized, preventing canonical LQG from reaching the physically correct quantum domain.

In this Letter, we introduce the first numerical approach implementing the Hamiltonian-constraint action on 3- and 4-valent SNs, the simplest duals to triangulations of bi- and tri-dimensional hypersurfaces (“spacetime cuts”), without recurring to its truncation to fixed graphs as is common in LQG. Our approach allows

for controlled recursive application of the Hamiltonian on SNs, yielding perturbative expansions of constraint-generated operators. A key feature of our approach is a bijective map between SNs and functions of lists, on which the Hamiltonian acts as a functional. The applicability of this approach might reach beyond LQG. All formulas derived and implemented are presented in the companion paper [19]. For the 3-valent case, akin to Ref. [20], our derivations update those in Refs. [21, 22], that employed the (outdated) Temperley-Lieb algebra [15] (leading to different results). Furthermore, building on and correcting the partial derivations from Ref. [23], we provide the first action of the Hamiltonian on 4-valent SNs.

We perform the first numerical study of graph-changing (GC) canonical LQG, computing volume expectation values of two perturbatively transformed 4-valent SNs. We compare the results with data generated with a graph-preserving (GP) Hamiltonian, presenting the first concrete indication that the latter fails to capture the proper SN dynamics. Our results on GC dynamics provide the missing reference point for approximations to be devised and tested, and should enable certain calculations to be performed entirely approximation-free. Lastly, considering that no eigenstates are known in the chosen algebra without additional assumptions, we find solutions to the Hamiltonian constraint with our code [24–26]. Performing GC computations opens a range of possibilities, including checks about how GC formulations affect semi-classical predictions [27, 28].

Using Ashtekar-Barbero variables [29–31], the Einstein-Hilbert action can be recast as smearings over 3 sets of constraints corresponding to gauge invariance, diffeomorphism invariance and (Euclidean) time reparametrization [32]. The resulting constrained system can be quantized “à la Dirac” [33, 34]. In the

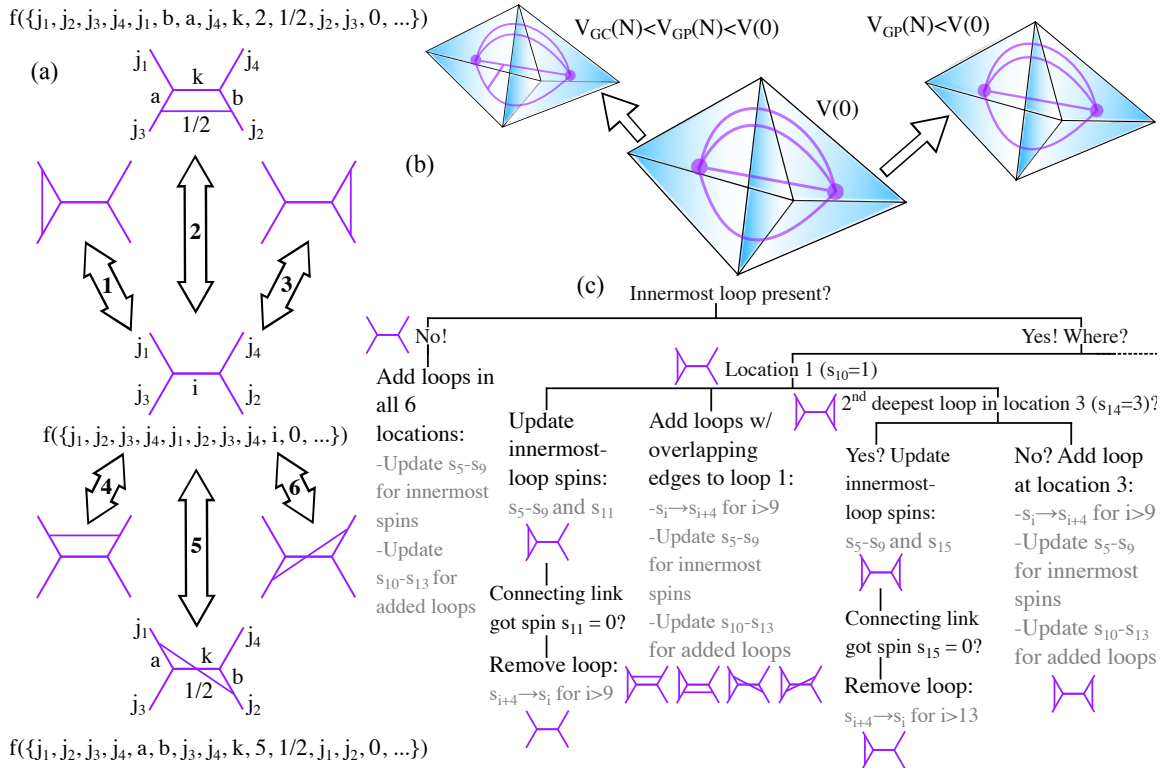


FIG. 1. (a) A 4-valent SN node (center), with its assigned ghost function below, transforms under the action of the Hamiltonian to give six modified structures containing inner loops (top and bottom). Ghost functions containing the lists encoding two such SNs, the top-most and bottom-most ones, are given. Double arrows emphasize the reversible character of the Hamiltonian, and the numbers within them highlight the location of the added loop. (b) Example of SN: the dipole model. Two 4-valent nodes are connected through their links pairwise, so that its dual is formed by two tetrahedra with faces that are pairwise glued (in 4D). These tetrahedra represent quanta of volume in a discretized geometry. Under the action of a unitary formed by exponentiating the Hamiltonian with a perturbation parameter  $N \ll 1$ , the transformed SN behaves differently when GC (left) or GP (right) dynamics are considered. (c) Pseudocode for the Hamiltonian implementation. The code checks whether an inner loop is present. If absent, it will introduce inner loops in all six locations, with spin 1/2 on the newly created link. If present, for each possible location, a series of steps is followed (the case for location 1 is shown, while for other locations the dashed-line continuation of the diagram implies similar rules not displayed). Namely, coupling a new loop at the innermost-loop location merely shifts spins without graph changes. If the connecting link reaches spin 0, it is removed, and the inner-loop data in the corresponding list is shifted left by 4 entries. Also, inner loops are added (deeper) to all other positions, but if a loop was added at position 3 right before inserting one at position 1 (these loops share no links), it either removes its extra link or simply changes spins. The diagram contains examples for the simplest SN for which the rules apply.

quantum theory, consideration solely of SNs with spin singlets at every node (also called intertwiners) suffices to satisfy the gauge constraint, which enforces fulfillment of the Cauchy-Schwarz inequalities. For SNs embedded in manifolds, diffeomorphisms can be understood as (invertible analytic) deformations of the graphs. To satisfy the diffeomorphism constraint, one considers equivalence classes of (dual) SNs with respect to diffeomorphisms [33, 35]: all graphs related by deformations should be superposed. The last constraint, referred to as Hamiltonian (or scalar constraint), dictates the dynamics. When neither matter nor a cosmological constant are considered, the simultaneous solutions to all constraints provide the physical states of LQG.

We consider the following (Hermitian) Hamiltonian:

$$\hat{C}_s = \lim_{\square \rightarrow 0} \sum_{\square} \frac{iN \epsilon_{ijk}}{3l_0^2} \text{tr} \left\{ \hat{h}[\alpha_{ji}] - \hat{h}[\alpha_{ij}], \hat{h}[p_k] \hat{V} \hat{h}^{-1}[p_k] \right\}. \quad (1)$$

Braces denote the anticommutator and  $\text{tr}$  the trace. The building blocks of Eq. (1) are the volume operator  $\hat{V}$  and the holonomies  $\hat{h}[p]$  (link-related parallel-transport unitaries) defined over a path  $p$ . The symbol  $\square$  represents a partition of the manifold into cubes, with cube sizes going to zero,  $\square \rightarrow 0$ , while their number diverges. As a result of this regularization, only the cubes centered at SN nodes contribute and no cube contains more than one node. The prefactor  $N$  is the lapse, serving as an amplitude modulator for the constraint action

in each cube. Here, we consider it independent of the cube. It translates a tridimensional foliation of space-time (or triangulation thereof) along a timelike vector of norm  $\propto N$ . The loops  $\alpha_{ij}$  and  $\alpha_{ji}$  of opposite orientations (i.e.,  $\alpha_{ij} = \alpha_{ji}^{-1}$ ) are formed by segments parallel to two perpendicular links (labelled by  $i$  and  $j$ ), connected by an additional link [the source of the GC effect, see Fig. 1(a)]. Path  $p_k$  is a line segment parallel to yet another link from the node (labelled  $k$ ), perpendicular to both  $i$  and  $j$  links. The totally anti-symmetric symbol  $\epsilon_{ijk}$  enforces that only holonomies applied over 3 mutually perpendicular links from an intertwiner contribute to the scalar-constraint action. These holonomies couple additional spins to SN links acted upon by  $\hat{C}_s$ . Lastly, the volume operator gives the number of (Planck-scale) quanta of volume based on the spins of the links connected to nodes of valency 4 or higher, with  $l_0$  being the Planck length. This provides an interpretation of SNs as duals to triangulations of manifolds, associating a link to each face of the triangulation, and a node to each tetrahedron [see Fig. 1(b)].

Graphical data can be rather unpractical and resource-consuming, yet transforming SNs demands the storage of information about superpositions of different (changeable) graphs with spins assigned to their links. Our goal is to encode SNs while allowing them to assume increasingly more complex structures resulting from loops added by the Hamiltonian closer and closer to the central nodes. We consider either 3 or 4 external legs (the outermost links). Their internal structures can accommodate an arbitrarily large number of inner loops ordered by their proximity to the central nodes. The spin and location information is stored as ordered lists, each in one-to-one relation with an SN. Since one cannot span a vector space out of lists, we construct a vector space of abstract functions for which the arguments are these lists. We call them ghost functions because they are never assigned a functional form. All needed information is in their arguments, which can have arbitrary size. Their orthogonality is based on whether arguments coincide: if  $s_i = \{s_{i,1}, s_{i,2}, \dots\}$  denotes lists encoding SNs, the functions  $f(s_i)$  are endowed with the inner product  $I[f(s_i), f(s_j)] = \delta_{i,j}$ . The Hamiltonian is then coded as a linear functional acting on the ghost functions by reading and manipulating their arguments:  $C_s[f(s_i)] = \sum_j c_j(s_i) f(s_j)$  for coefficients  $c_j$  taken from the action of Eq. (1) on 3-valent or 4-valent SNs and derived in the companion paper [19]. Linearity implies  $C_s[\sum_i c_i f(s_i)] = \sum_i c_i C_s[f(s_i)]$ , thus the constraint functional can be used recursively.

We focus here on 4-valent SNs with 4 external legs, an inner virtual link and an arbitrary number of inner loops. The inner loops can be arranged in 6 different ways, by connecting links belonging to each possible pair of directions [cf. Fig. 1(a)]. We label such inner-loop locations from 1 to 6, connecting links along the respective

pairs  $\{p_1, p_3\}$ ,  $\{p_2, p_3\}$ ,  $\{p_2, p_4\}$ ,  $\{p_1, p_4\}$ ,  $\{p_1, p_2\}$ , and  $\{p_3, p_4\}$ . In the central SN of Fig. 1(a),  $j_i$  is the link spin along direction  $p_i$ . The presence of certain inner loops affects the manner in which Eq. (1) can attach new loops. If a loop is present, e.g., in location 1 (placed between directions  $p_1$  and  $p_3$ ),  $C_s$  attaches a new loop in the same location by coupling its holonomies with the already existing loop links, without changing the graph structure, but altering the spins of these links (unless the spin of the connecting link becomes zero, changing the graph). The Hamiltonian also forms inner loops in all other locations, but the presence of a loop in location 1 means that loops in locations 2, 4, 5, and 6 (sharing a common link with loop 1) would have to be introduced further inwards relative to the location-1 loop. Meanwhile, a loop introduced in location 3 is unaffected by that loop and could be located at similar depth. Consequently, recursive application of Eq. (1) generates structures with increasingly deeper inner loops, with depths dependent on loop positions. Figure 1(c) shows pseudocode exemplifying the addition/removal of loops.

Our SN-encoding lists have the spins of the outermost links as their first four entries. They are stored only for normalization. The next four entries are the innermost spins adjacent to the central virtual link, i.e., along directions  $p_1, p_2, p_3$ , and  $p_4$ . The 9th entry is the central-virtual-link spin. If the SN has no inner loops, all remaining entries are zero [cf. center of Fig. 1(a)]. Otherwise, the innermost-loop data occupy the next 4 entries, and every following loop, in decreasing order of depth, is described by 4 additional entries: the first two store the location of the loop and the spin of its connecting link, while the other two store the spins adjacent to (but not contained in) the loop along the directions it connects. When  $C_s$  creates a new loop, it moves all entries from 10th onward to the right by 4, so that inner-loop entries are moved down in depth order to allow for inclusion of the new-loop data. The new spins adjacent to the central nodes are encoded in entries 5-8, and the new central spin in the 9th entry. Information about the added innermost loop occupies entries 10-13. Although SNs and their encoding lists become increasingly complex,  $\hat{C}_s$  acts only upon the two deepest inner loops of a 4-valent SN. Since we store the information about these two loops between the 5th and 17th entries, the coefficients  $c_j(s_i)$  in  $C_s[f(s_i)] = \sum_j c_j(s_i) f(s_j)$  depend only on these entries of the input-ghost-function argument, avoiding the search for entries scattered among large lists.

The constraint is a map between nonnormalized SNs. So, normalization is required after applying  $C_s$  several times. The “normalizer” functional linearly implements this according to  $f(s_i) \rightarrow [d_{j_1} d_{j_2} d_{j_3} d_{j_4} \prod_k d_k^{-1}] f(s_i)$  [19], where  $d_j = 2j + 1$ . Here,  $j_i$  are spins of the outermost legs and  $k$  runs over the spins of all SN links, including the outermost ones. To achieve this, the normalizer reads in each ghost-function argument the first 6 entries and the

$j$ th,  $(j-1)$ th, and  $(j-2)$ th entries for  $j = 4n+9$  ( $n \in \mathbb{N}$ ).

As key observable, we implement a quantum-volume functional. It only sees the spins adjacent to the central link in the SN. These determine the size of the matrix generated by the volume operator. Since the volume maps a 4-valent SN with central spin  $i$  into a linear combination of 4-valent SNs with all possible central spins, the size of the matrix it generates runs from  $\min\{|j'_1 - j'_3|, |j'_2 - j'_4|\}$  to  $\max\{j'_1 + j'_3, j'_2 + j'_4\}$  (for innermost spins  $j'_1, j'_2, j'_3$ , and  $j'_4$ ), and the indices are the input and output central-link spin values. The volume is derived from an intermediate operator acting on the SNs, whose matrix needs to be diagonalized, so that the absolute value and square root of its entries can be taken before the inverse of the diagonalizing transformation is applied, giving volume-operator matrix elements in a basis of 4-valent-SN states [19]. Finally, the inner-product functional is defined by linearity as  $I[\sum_i c_i f(s_i), \sum_j d_j f(s_j)] = \sum_{i,j} c_i^* d_j I[f(s_i), f(s_j)]$ .

The solutions to constraint (1), which compose the space of physical states in LQG, remain unknown. Some solutions were found (a) in the presence of a semi-classical massive scalar field [24], (b) using the Temperley-Lieb al-

gebra [25] and (c) using an incomplete Hamiltonian [23], yet none holds in the case we study. The existence of certain classes of diffeomorphism-invariant solutions was also proven, but no explicit solution was constructed [26]. Using our code, we have searched for states annihilated by  $\hat{C}_s$ . Our protocol runs over semi-integer spins within  $[0, 7/2]$  on each link of an SN without inner loops. Only gauge-invariant states are allowed. Within the investigated spin range, we have found a solution only for  $j_1 = j_2 = j_3 = j_4 = i = 0$ , suggesting that SNs with zero innermost spins connected to the intertwiners provide solutions. When acting on a linear combination of SNs that cannot be generated from one another by inner-loop couplings, the Hamiltonian generates a linear combination of SNs that does not overlap with the input state  $|s_0\rangle$ . Denoting as  $|s_i\rangle$  the state generated by  $i$  loop insertions on  $|s_0\rangle$ , with  $\langle s_i | s_j \rangle = \delta_{ij}$  and  $\hat{C}_s |s_0\rangle = c_1^* |s_1\rangle$ , we have  $\hat{C}_s |s_i\rangle = c_i |s_{i-1}\rangle + c_{i+1}^* |s_{i+1}\rangle = \langle s_{i-1} | \hat{C}_s |s_i\rangle |s_{i-1}\rangle + \langle s_{i+1} | \hat{C}_s |s_i\rangle |s_{i+1}\rangle$ . Therefore, from  $|s_0\rangle$ , we can generate the following solution to our Hamiltonian constraint [19]:

$$|E_0\rangle = |s_0\rangle - \frac{\langle s_1 | \hat{C}_s |s_0\rangle}{\langle s_1 | \hat{C}_s |s_2\rangle} |s_2\rangle + \frac{\langle s_1 | \hat{C}_s |s_0\rangle \langle s_3 | \hat{C}_s |s_2\rangle}{\langle s_1 | \hat{C}_s |s_2\rangle \langle s_3 | \hat{C}_s |s_4\rangle} |s_4\rangle + \dots = \sum_{i \text{ even}} (-1)^{i/2} \frac{\langle s_1 | \hat{C}_s |s_0\rangle}{\langle s_1 | \hat{C}_s |s_2\rangle} \dots \frac{\langle s_{i-1} | \hat{C}_s |s_{i-2}\rangle}{\langle s_{i-1} | \hat{C}_s |s_i\rangle} |s_i\rangle. \quad (2)$$

We now investigate the validity of the GP approximation commonly used in the literature. By perturbatively transforming SNs, we estimate how the expectation value of the volume transforms when comparing GC and GP dynamics. We consider  $N$  as our perturbation parameter, and expand the unitary  $\hat{U} = \exp[-i\hat{C}_s(N)]$  [36] up to 3rd and 4th order for GC and GP scenarios, respectively. Note that odd-order contributions to expectation values of observables are absent in our calculations. Since, under the action of the GC constraint, any SN graph can only be recovered after applying the constraint an even number of times, while the volume operator does not change graphs,  $\langle \hat{C}_s^n \hat{V} \hat{C}_s^m \rangle = 0$  for  $n+m$  odd. This also holds for Hamiltonian matrix elements, with  $\langle \hat{C}_s^m \rangle = 0$  for  $m$  odd. For fixed graph structures, however, an SN can be recovered after an odd number of applications of the Hamiltonian, depending on the SN connectivity [19]. We consider a ladder-type SN with intertwiners connected by their upper or lower pairs of legs and loop couplings restricted to solely happen above and below the fiducial intertwiner, neglecting large loops coupled from the sides (which can lead to  $\langle \hat{C}_s^m \rangle \neq 0$ ,  $\langle \hat{C}_s^n \hat{V} \hat{C}_s^m \rangle \neq 0$  for  $m$  odd).

The volume expectation value as a function of the lapse  $N$  for two fiducial SNs is shown in Fig. 2. We choose the

central SN in Fig. 1(a) with  $j_1 = j_2 = j_3 = j_4 = 1/2$  and  $i = 0$  (red curves) or  $i = 1$  (green curves). Unexpectedly, the curves coincide for the two SNs transformed under GC dynamics. The results indicate that the GP approximation leads to miss-estimation of this geometric observable. The volumes surprisingly decrease with  $|N|$  for  $|N| \lesssim 1/2$ . For the GP case, the volume actually increases when  $|N| \gtrsim 1/2$  due to 4th-order contributions, and a similar trend is expected for GC dynamics. This represents the first quantitative evidence that GP approximations lead to departure from the GC dynamics. Furthermore, the fact that  $\langle \hat{C}_s^m \rangle \neq 0$  can happen in the GP case for  $m$  odd, leading to asymmetries in the volume dependence on  $N$ , further evidences the severe effects of this approximation.

Our work introduces a numerical tool to solve problems involving large superpositions of (changing) graphs. We use it for first GC calculations in canonical LQG, providing quantitative data for the volume, which shows that the dynamics of GP Hamiltonians depart from the correct GC one. We also introduce new families of potential solutions to the GC Hamiltonian. Lastly, we have for the first time derived the complete action of the Hamiltonian on 4-valent SNs, with details given in Ref. [19]. Our work enables a new generation of LQG calculations in which

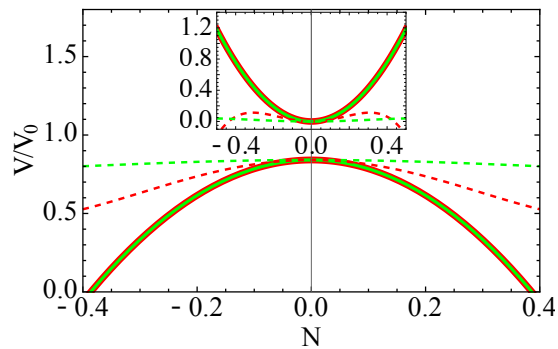


FIG. 2. Variation of the dimensionless quantum-volume expectation value with the lapse. The curves are shown for two SNs with  $j_1 = j_2 = j_3 = j_4 = 1/2$ ,  $\varepsilon = 0$ , and either  $i = 0$  (red) or  $i = 1$  (green). We compare GC (solid) and GP Hamiltonians (dashed), for which unitaries are expanded up to 3rd and 4th order in  $N$ , respectively. Inset: corresponding curves for the volume variances.

approximations are either avoided or better controlled, allowing for studies of observable properties of quantum geometries, which could eventually be measurable in future experiments [37, 38] or quantum simulations.

*Acknowledgements.*—The authors are grateful for discussions with and suggestions by Ilkka Mäkinen, Jorge Pullin, Carlo Rovelli, and Etera Livine.

FV’s research at Western University has been supported by the Canada Research Chairs Program and by the Natural Science and Engineering Council of Canada (NSERC) through the Discovery Grant “Loop Quantum Gravity: from Computation to Phenomenology.” She has also been supported by the ID# 62312 grant from the John Templeton Foundation, as part of the project “The Quantum Information Structure of Spacetime” (QISS). FV acknowledges the Anishinaabek, Haudenosaunee, Lūnaapēwak, Attawandaron, and neutral peoples, on whose traditional lands Western University.

TLMG and MM acknowledge support by the ERC Starting Grant QNets through Grant Number 804247, and the European Union’s Horizon Europe research and innovation program under Grant Agreement Number 101114305 (“MILLENION-SGA1” EU Project) and under Grant Agreement Number 101046968 (BRISQ). MM furthermore acknowledges support by the Deutsche Forschungsgemeinschaft (DFG, German Research Foundation) under Germany’s Excellence Strategy ‘Cluster of Excellence Matter and Light for Quantum Computing (ML4Q) EXC 2004/1’ 390534769. This research is also part of the Munich Quantum Valley (K-8), which is supported by the Bavarian state government with funds from the Hightech Agenda Bayern Plus.

GAMM acknowledges support by MCIN/AEI/10.13039/501100011033/FEDER from Spain under the Grant Number PID2020-118159GB-C41 and also partly by the Grant Number PID2023-149018NB-C41, funded

by MCIU/AEI/10.13019/501100011033 and by FSE+.

\* t.guedes@fz-juelich.de

† mena@iem.cfmac.csic.es

‡ fvidotto@uwo.ca

§ markus.mueller@fz-juelich.de

- [1] C. Rovelli and L. Smolin, Discreteness of area and volume in quantum gravity, *Nucl. Phys. B* **442**, 593 (1995).
- [2] P. Doná, M. Han, and H. Liu, Spinfoams and High-Performance Computing, *Handbook of Quantum Gravity*, edited by C. Bambi, L. Modesto, and I. Shapiro, (Springer Nature, Singapore, 2022).
- [3] A. Courtney, F. Girelli, and S. Steinhaus, Numerical evaluation of spin foam amplitudes beyond simplices, *Phys. Rev. D* **105**, 066003 (2022).
- [4] F. Gozzini, A high-performance code for EPRL spin foam amplitudes, *Class. Quantum Grav.* **38**, 225010 (2021).
- [5] M. Han, H. Liu, and D. Qu, A Mathematica program for numerically computing real and complex critical points in 4-dimensional Lorentzian spinfoam amplitude, [arXiv:2404.10563](https://arxiv.org/abs/2404.10563) (2024).
- [6] S. K. Asante, B. Dittrich, and S. Steinhaus, Spin Foams, Refinement Limit, and Renormalization, *Handbook of Quantum Gravity*, edited by C. Bambi, L. Modesto, and I. Shapiro, (Springer Nature, Singapore, 2022).
- [7] C. Rovelli and F. Vidotto, *Covariant Loop Quantum Gravity* (Cambridge University Press, Cambridge, 2014).
- [8] H. Sahlmann and W. Sherif, Towards quantum gravity with neural networks: Solving the quantum Hamilton constraint of U(1) BF theory, *Class. Quantum Grav.* **41**, 225014 (2024).
- [9] C. Rovelli and L. Smolin, The physical Hamiltonian in nonperturbative quantum gravity, *Phys. Rev. Lett.* **72**, 446 (1994).
- [10] R. Penrose, Angular momentum: an approach to combinatorial spacetime, in *Quantum Theory and Beyond*, edited by Ted Bastin (Cambridge University Press, Cambridge, 1971), page 151.
- [11] C. Rovelli and L. Smolin, Spin networks and quantum gravity, *Phys. Rev. D* **52**, 5743 (1995).
- [12] R. Koenig, G. Kuperberg, and B.W. Reichardt, Quantum computation with Turaev–Viro codes, *Ann. Phys. (N.Y.)* **325**, 2707 (2010).
- [13] Y.-J. Liu, K. Shtengel, A. Smith, and F. Pollmann, Methods for simulating string-net states and anyons on a digital quantum computer, *Phys. Rev. X Quantum* **3**, 040315 (2022).
- [14] S. Trebst, M. Troyer, Z. Wang, and A.W.W. Ludwig, A short introduction to Fibonacci anyon models, *Prog. Theor. Phys. Supp.* **17**, 384 (2008).
- [15] L.H. Kauffman and S. Lins, *Temperley-Lieb Recoupling Theory and Invariants of 3-Manifolds* (Princeton University Press, Princeton, 1994).
- [16] D.M. Brink and G.R. Satchler, *Angular Momentum*, 2nd edition (Clarendon Press, 1968).
- [17] A. Messiah, *Quantum Mechanics Vol. II* (North Holland Publishing Company, Amsterdam, 1962).
- [18] I. Mäkinen, Introduction to SU(2) recoupling theory and graphical methods for loop quantum gravity,

- arXiv:1910.06821 (2019).
- [19] T.L.M. Guedes, G.A. Mena Marugán, M. Müller, and F. Vidotto, companion paper, Taming Thiemann’s Hamiltonian constraint in canonical loop quantum gravity: Reversibility, eigenstates and graph-change analysis, arXiv:2412.XXXXX (2024).
- [20] J. Yang and Y. Ma, Graphical calculus of volume, inverse volume and Hamiltonian operators in loop quantum gravity, *Eur. Phys. J. C* **77**, 1 (2017).
- [21] R. Borissov, R. De Pietri, and C. Rovelli, Matrix elements of Thiemann’s Hamiltonian constraint in loop quantum gravity, *Class. Quantum Grav.* **14**, 2793 (1997).
- [22] M. Gaul and C. Rovelli, A generalized Hamiltonian constraint operator in loop quantum gravity and its simplest Euclidean matrix elements, *Class. Quantum Grav.* **18**, 1593 (2001).
- [23] E. Alesci, T. Thiemann, and A. Zipfel, Linking covariant and canonical loop quantum gravity: New solutions to the Euclidean scalar constraint, *Phys. Rev. D* **86**, 024017 (2012).
- [24] M. Domagała, K. Giesel, W. Kamiński, and J. Lewandowski, Gravity quantized: Loop quantum gravity with a scalar field, *Phys. Rev. D* **82**, 104038 (2010).
- [25] R. Gambini, J. Griego, and J. Pullin, Chern-Simons states in spin-network quantum gravity, *Phys. Lett.* **B413**, 260 (1997).
- [26] T. Thiemann and M. Varadarajan, On propagation in loop quantum gravity, *Universe* **8**, 615 (2022).
- [27] M. Christodoulou and F. D’Ambrosio, Characteristic time scales for the geometry transition of a black hole to a white hole from spinfoams, *Class. Quantum Grav.* **41**, 195030 (2018).
- [28] H. Huang, J. Kunz, J. Yang, and C. Zhang, Light ring behind wormhole throat: Geodesics, images, and shadows, *Phys. Rev. D* **107**, 104060 (2023).
- [29] A. Ashtekar, New variables for classical and quantum gravity, *Phys. Rev. Lett.* **57**, 2244 (1986).
- [30] L. Smolin and C. Rovelli, Knot theory and quantum gravity, *Phys. Rev. Lett.* **61**, 1155 (1988).
- [31] J.F. Barbero G., Real Ashtekar variables for Lorentzian signature space-times, *Phys. Rev. D* **51**, 5507 (1995).
- [32] T. Thiemann, Anomaly-free formulation of non-perturbative, four-dimensional Lorentzian quantum gravity, *Phys. Lett.* **B380**, 257 (1996).
- [33] A. Ashtekar and J. Lewandowski, Background independent quantum gravity: A status report, *Class. Quantum Grav.* **21**, R53 (2004).
- [34] P.A.M. Dirac, *Lectures on Quantum Mechanics* (Yeshiva University, New York, 2001).
- [35] C. Rovelli, *Quantum Gravity* (Cambridge University Press, Cambridge, U.K., 2004).
- [36] M.P. Reisenberger and C. Rovelli, “Sum over surfaces” form of loop quantum gravity, *Phys. Rev. D* **56**, 3490 (1997).
- [37] C. Rovelli, Planck stars as observational probes of quantum gravity, *Nature Astron.* **1**, 0065 (2017); Correction, *Nature Astron.* **1**, 0097 (2017).
- [38] A. Ashtekar, B. Gupt, D. Jeong, and V. Sreenath, Alleviating the tension in the cosmic microwave background using Planck-scale physics, *Phys. Rev. Lett.* **125**, 051302 (2020).